# HOOD VENTILATION-RATE EFFECTS ON FIRE STRUCTURES IN A COMPARTMENT

**Wu-Chi Ho, Ling-Chia Weng**
Center for Aviation and Space Technology
Industrial Technology Research Institute
Chutung, Hsinchu, Taiwan 310
R.O.C.

**Chiun-Hsun Chen**
Department of Mechanical Engineering
National Chiao-Tung University
Hsinchu, Taiwan 300
R.O.C.

## ABSTRACT

This paper applies a commercial field-model code, CFX, to predict the ISO 9705 compartment fires for three different ventilation rates. The predicted results generally agree well with the corresponding experimental data. The ventilation intensity changes the flow path of entrained air and flow structure on the doorway plane to affect the fire structure inside the compartment and mass flow rate across the doorway. There exist many recirculation cells in the compartment to facilitate the mass and heat transfer. The temperature stratification phenomenon is found away from the burner. The thinnest hot layer is observed in the ventilation rate of 2 kg/s.

## INTRODUCTION

The present simulation, using a field model, studies the effects of the forced ventilation rates on the fire behaviors in the ISO 9705 room fire test. The motivation is that the test instrumentation mentioned in the above standard test cannot provide the detailed flow field structures inside the room, whereas a numerical simulation, if accurate enough, may give valuable insights of the corresponding combustion characteristics via a parametric study.

The application of a field model on the fire simulation has gradually gained much more attention recently in comparison with that of zone model, because its physical features can provide the detailed flow and thermal structures in a compartment fire especially when mixing and/or ventilating rates are significant; see References 1–6 for examples. Lockwood and Malalasekera[1] applied a field model to predict the compartment fires. Their computational results were compared with the experimental data from two laboratories. On the whole, the agreement was good. However, they concluded that more measurements and a sophisticated sub-model for flame spread are needed in order to accurately predict the fire behaviors. Chow and Leung[2] modified the source terms in $\kappa$ and $\epsilon$ transport equations, which are part of the field-typed governing equations, to let both values of $\kappa$ and $\epsilon$ to not be negative. In such treatment, the convergent numerical results can be achieved to properly predict the fire phenomena inside a building at the preflashover stage. Hadjisophocleous and Cacambouras[3] developed a transient, three dimensional and turbulent field model to simulate a fire inside an enclosure, whose heat source was treated as a linear function of time. The comparison between the experimental data and computed results showed that they were in reasonable agreement. Chow and Fong[4] studied the interaction between the sprinkler and fire-induced smoke layer numerically. The smoke in the gas phase was simulated by using a field model, whereas the droplet motion from the sprinkler was described by Newton's second law with an air drag and the droplet itself was subjected to convective heat transfer from the smoke layer. However, they just visualized the interaction between the air-flow pattern, temperature

and droplet properties without considering the fire and suppression effects. Kerrison *et. al.*[5] applied two CFD commercial codes, PHOENICS and FLOW3D (now named as CFX), respectively, to study the fire induced flows in rooms. A set of comparisons based on the measured and predicted temperature and velocity profiles at three different doorways were given. They concluded that both models can give the same reasonable trend as that in experimental results. Habib and Jaluria[6] numerically studied a compartment fire in an enclosure with an opening. They found that the stratification level strongly affects the characteristics of the thermal plume above the fire. Also a multi-cellular pattern appears in the flow-field which could distort the two-layer assumption used in the zone model.

The works mentioned above mostly emphasized the natural convective flow induced by the compartment fire. It is, therefore, appropriate to expand the computational domain into the quiescent atmosphere outside the compartment openings, such as References 1 and 5. On the other hand, if the simulation is based on the ISO 9705 standard room-corner test, where an exhaust hood is employed just outside and adjacent to the top of doorway to collect combustion product gases and smoke, the downstream boundary conditions of the opening should be significantly affected by the forced ventilation from this apparatus. Therefore, the computational domain should be able to cover the interaction of the forced ventilation and air-flow into the fire room. It seems few efforts have considered such an influence on the fire behaviors of the ISO 9705 test which motivates this study.

The objective of the present numerical study is to investigate the effects of forced ventilation on the turbulent reacting flow inside an ISO 9705 fire compartment. In order to simulate the flow field correctly, the compartment, exhaust gas hood and surrounding atmosphere should be included in the computational domain so that the precise boundary conditions of the problem can be provided. The simulation, using CFX[7], is based on Wang's experiments[8], which fully complied with the ISO 9705 standard. A comparison between the numerical and experimental results will be given first in order to verify that the calculations simulate the experiments. Then, the numerical results by a series of parametric studies will demonstrate the impact of the ventilation mass flow rate on the compartment fire characteristics, such as the mass transfer through the opening, the velocity profiles across the doorway plane, the flow structures and temperature distributions inside the compartment, etc.

## Mathematical Model

The formulation of the differential equations describing the fire will not be given here because they can be found elsewhere[7,9]. The simulation is embodied in the solution of the balance equations for three velocity components, the enthalpy, the mixture fraction, the turbulent kinetic energy and the dissipation rate of the turbulence energy. Since the buoyant force plays a dominant role on the flow structure in compartment fires, the k-$\epsilon$ turbulence model with a buoyancy modification[7] is used. The constants used in the present model are the same as those in the standard k-$\epsilon$ model[3]. The fire source is simulated by a propane gas burner, exactly the same as that used in the experimental work[8], therefore, a mixed-is-burnt combustion model[9] is applied to describe the turbulent diffusion flame created. The mean mass fractions of fuel, oxidant and product are obtained from the mean and variance of the mixture fraction using an assumed form for the probability density function (PDF). The double delta PDF is adopted here. These equations have a common form, which can be expressed in Cartesian tensor notation as:

$$\frac{\partial}{\partial t}(\rho\phi) + \frac{\partial}{\partial x_j}(\rho u_j \phi) = \frac{\partial}{\partial x_i}\left[\Gamma_\phi \frac{\partial \phi}{\partial x_j}\right] + S_\phi$$

where $\phi$ represents the respective variable mentioned above, $\Gamma$ the corresponding effective exchange coefficient of $\phi$, and $S_\phi$ the source term. The hybrid-differencing technique is employed for convective terms, and the central differencing technique is employed for others. The resultant discrete equations are solved iteratively by the SIMPLEC algorithm developed by Van Doormaal and Raithby[10].

## Numerical Details

Figure 1 shows the geometric configuration of the computational domain used in this simula-

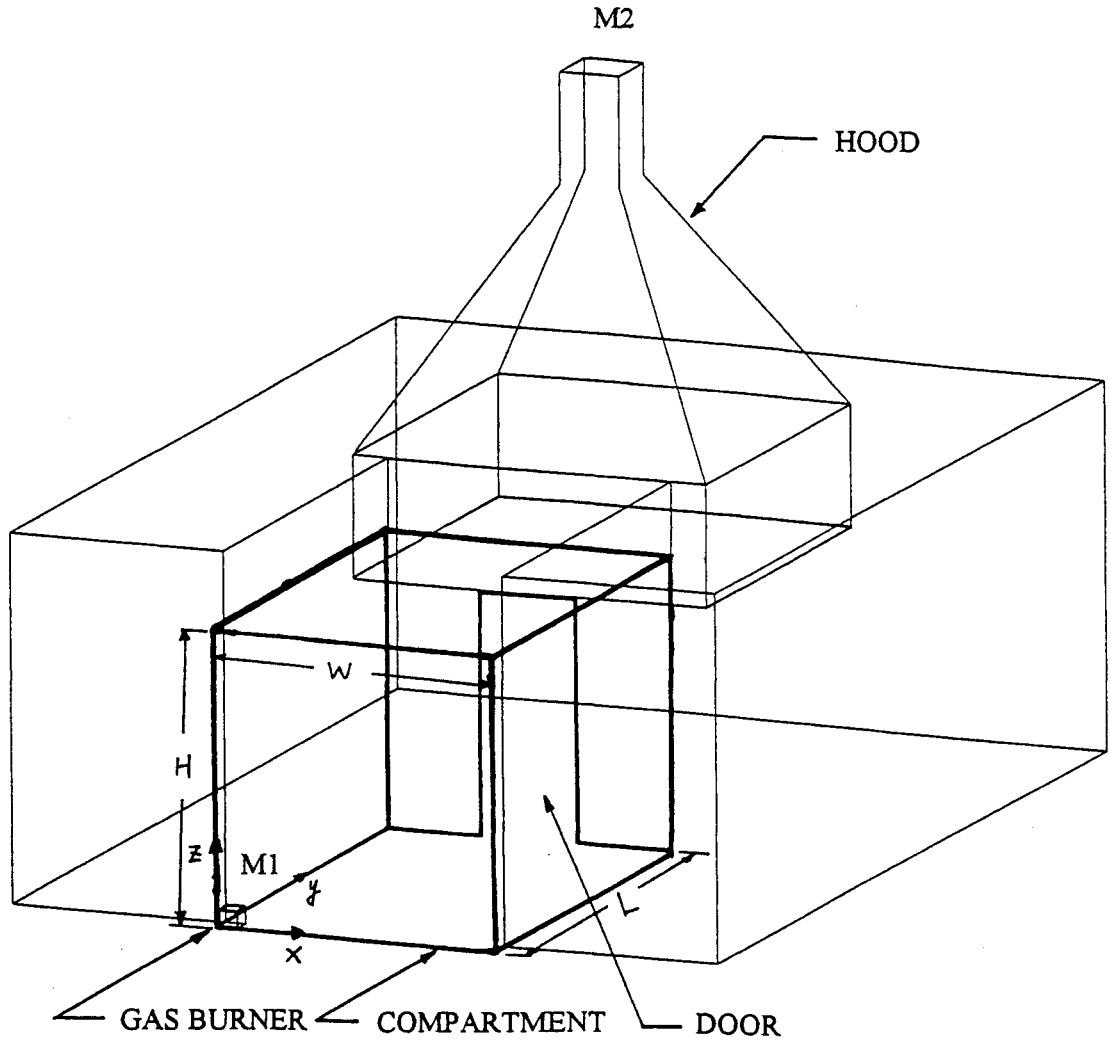


Figure 1. The Computational Domain.

tion. The computational domain consists of three sub-regions, which are the compartment, hood and atmosphere regions, respectively. The compartment has a single opening (doorway), hence, its downstream flow conditions determine the exchange rates of mass and heat as well as the fire structures inside the compartment. Therefore, the computational domain should be expanded in all directions. The geometry, numerical grid, boundary conditions, and convergence criterion are described as follows.

## Geometry

The compartment and hood scales in the numerical model are the same as those in the experiments of Wang[8]. The compartment is 2.4 m (L) × 2.4 m (W) in plane and 3.6 m (H) in height. A gas burner (0.17 m × 0.17 m) is placed in the corner, as shown in Fig. 1, and supplied with commercial grade propane at a fixed rate as in previous experiments[8]. The opening is 0.8 m in width and 2 m in height. To collect the combustion product gases and smoke emerging from the compartment, a 3 m × 3 m hood is placed adjacent to the sill of the doorway.

## Grid

The computational grid was constructed using a body-fitted, multi-block grid structure[7]. The grid system, shown in Fig. 2, is composed of 69,750 cells. Note that only 7,840 grid points are placed inside the compartment. In other words, only one-tenth of the grid points are used to describe the reacting flow features in the domain of interest. Although the computational solutions based on this rather coarse grid resolution might not be grid-independent, a finer grid system was not created due to the limitations of computer stor-

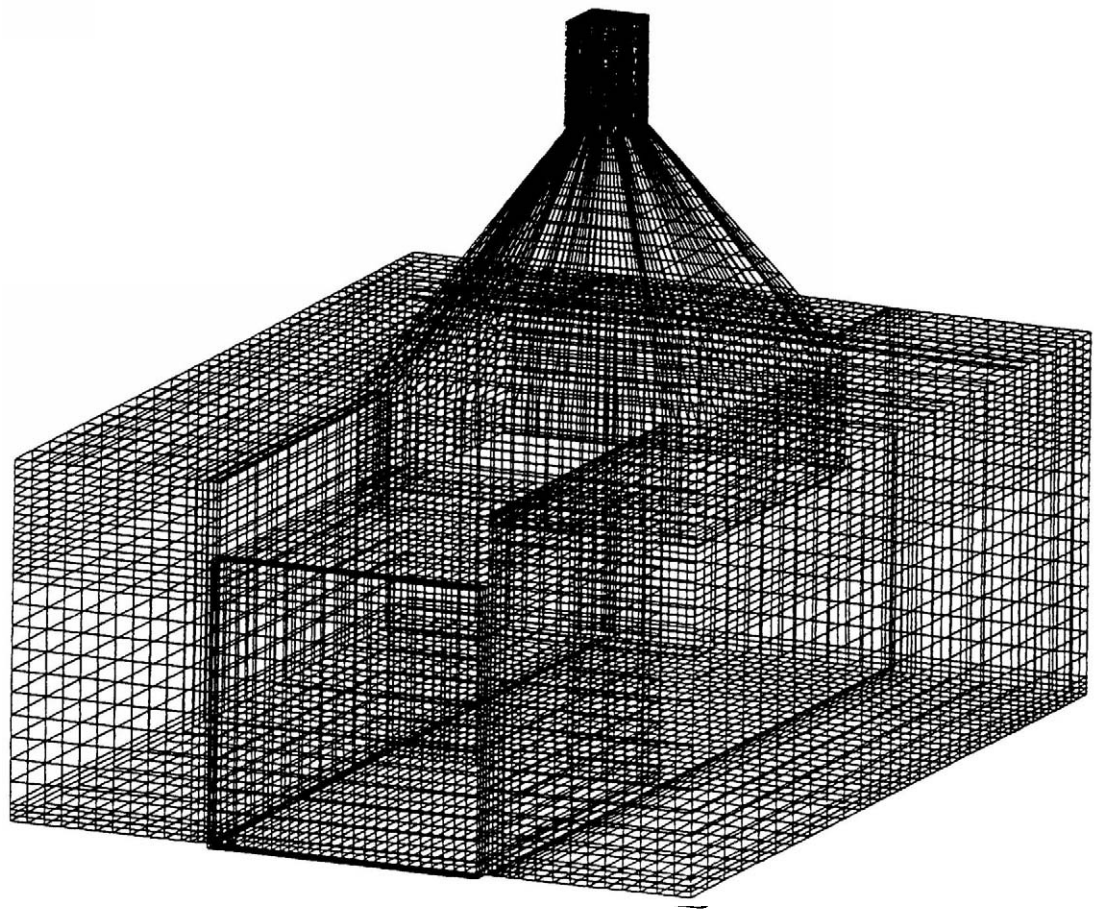

Figure 2. The Surface Grid Distribution.

age and executing time necessary to obtain a steady-state solution. According to the corresponding numerical experience for a similar flow problem by Kerrison *et al.*[5], who used FLOW3D (now CFX)[7], a grid refinement should improve the prediction accuracy. However, it is believed that the grid resolution generated in the present study was good enough to capture all the relevant flow characteristics.

## Boundary Conditions

A uniform velocity profile with a 3% turbulent intensity is assumed at the burner outlet. A zero gradient is prescribed at all free boundaries for all the variables. According to the numerical experience of similar flows[1], carefully formulated specifications of free boundaries do not always guarantee the convergence across a range of problem conditions. To secure computational stability, Lockwood and Malalasekera[1] calculated the free boundary conditions from individual mass balance; the velocities parallel to the plane were set to zero. In the present study, we chose the so-called "pressure boundary"[7] at the free boundary and do not employ any other special treatment. Sufficient grid cells are employed in the computational domain extending into the quiescent atmosphere, as mentioned previously. Since there are eight free surfaces in the computational domain, the numerical convergence problem appears if CFX is run in the steady-state mode[11]. This will be addressed in the following section. Adiabatic boundary conditions are assumed for all of the solid walls, which are made of gypsum boards in experiments[8]. To reduce the substantial core and computational time requirements, the near-wall region is handled by means of wall function prescription[5].

## Convergence

The calculation is terminated when the mass and velocity residuals are less than $1 \times 10^{-2}$. If CFX is run in steady-state mode, then these residuals are almost impossible to meet the prescribed level and, consequently, the numerical calculation may not be converged. On the other hand,

if CFX is run in a transient mode, a few-thousand time steps are required before reaching a steady-state condition. In addition to the mentioned convergence criteria, the mass residual of the flow across the doorway plane is used as well to judge the convergence status of the numerical results. If this mass residual variation is less than 5%, then the computation is terminated. Otherwise, the computation is continued for another 100 time steps.

The computation was carried out on an IBM RISC-6000 workstation. A typical computational case requires approximately 260 hours of computer time to obtain a steady-state solution.

## Results and Discussions

To explore the impact of forced ventilation on the fire structure in the compartment, three ventilation mass flow rates, Mv = 0.5, 1.0 and 2.0 kg/s, were selected in the parametric study. Mv = 2.0 kg/s is the one used in the experiment[8]. The burner is fueled by propane, which is preheated to 288 K. To meet the heat release rate prescribed in ISO 9705, the volumetric flow rate of propane is set at 65 L/min. It is equivalent to an output heat flux of 100 kW. This simulation is executed up to a steady-state solution in the regime of a 100 kW energy supply rate only, and does not simulate the following 300 kW regime in the latter ten-minute period in the experiment[8] as required by ISO 9705. Therefore, the comparisons are based on the measured data of Wang's experiments[8] at the end of ten minutes.

### Comparisons with experimental measurements

In order to examine the prediction capability of the numerical model when used for the simulation of the compartment fire under a forced ventilation environment, the numerical results are first compared with the available experimental data[8]. Wang[8] carried out a series of compartment fire tests using the specified heat release rates from the burner and the different wall materials. Figure 3 gives a comparison of the measured and calculated velocity profiles at the center of the doorway for a ventilation flow rate of 2 kg/s. The computed velocity profiles for ventilation rates of 0.5 and 1.0 kg/s are also shown in this figure. It can be seen that the predicted velocities for a

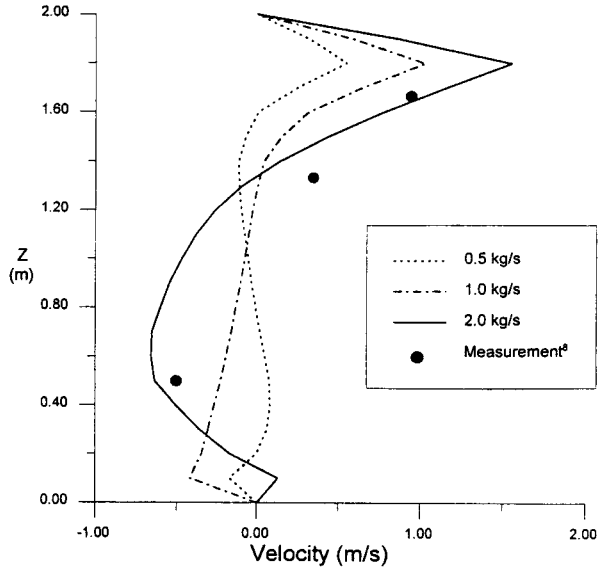


Figure 3. Vertical Velocity Profiles at the Center of Doorway.

flow rate of 2 kg/s are quite close to the ones at the three measured points located in the inflow and outflow regions. We expect that further improvement of the prediction can be achieved by increasing the grid resolution inside the compartment, as reported in Kerrison *et al.*[5]

Figure 4 shows the comparison between the predicted and measured vertical temperature distributions in the corner location inside the compartment. The predicted values of temperature are in general good agreement with the measured

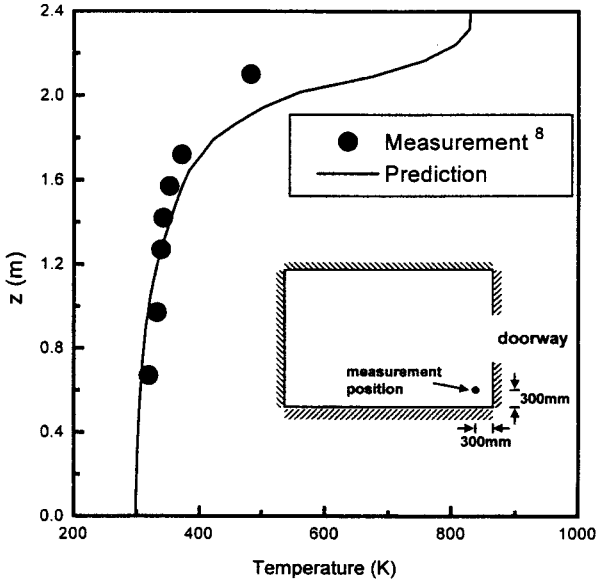


Figure 4. Predicted and Measured Vertical Temperature Profiles in the Compartment.

ones, except the one near the bottom of the hot layer. It may be caused by two reasons. First, it may be the result of an insufficient grid resolution in the present calculation. Secondly, the present simulation does not consider the radiation heat loss and the conduction heat losses to walls and ceiling (the adiabatic boundary conditions are assumed in these places). It is strongly believed that the latter is the main reason contributing to the over-estimated temperature distribution in the hot layer beneath the ceiling which can be confirmed by References 3 and 12. The predicted neutral layer height is found lower than the one in the measurement[8]. According to the finding of Kerrison *et al.*[5] and Lewis *et al.*[12], an increase of the gird resolution will lead to an increase of the neutral layer height. On the other hand, the measurement uncertainty in the experiments[8] cannot be excluded as a possible source for inducing the over-estimation phenomenon in the calculations. From the above comparisons, we are confident that the present model can properly construct the fire structures inside the fire compartment. Finally, a layered structure is predicted here. It was also mentioned in Reference 12, which distributed the heat release through the introduction of a combustion model.

## Flow Characteristics on the Doorway Plane

Returning to Fig. 3, it clearly demonstrates the significant influence of the ventilation flow rate on the flow characteristics across the doorway plane. In general, an outflow region can be distinguished from an inflow region for the larger ventilation rates, such as 1.0 and 2.0 kg/s. On the other hand, it becomes a little more complicated for the case of Mv = 0.5 kg/s. The corresponding numerical results of isothermal (cold) cases in a preliminary study reported by Ho *et al.*[11] showed that a small inflow region is generated near the top of the doorway even for the case of Mv = 2.0 kg/s due to the local recirculation flow motion. However, in the same region only an outflow pattern is found in the present chemical reacting compartment flows, as shown in this figure. Apparently, the local recirculation flow is suppressed by the strong upward flow motion, resulting from the strong buoyancy force due to combustion.

Figure 5 shows the contours of the normal velocity component on the doorway plane. They also indicate that the distributions of the inflow (dash lines) and outflow (solid lines) regions are significantly affected by the ventilation flow rate through the gas hood. In the isothermal cases[11], the basic structures of inflow and outflow regions remain unchanged with the ventilation rates, although their size and strength are varied accordingly. Apparently, the forced ventilation rate contributes to the stronger effects on the flow structure of the doorway plane in the combustion cases. As Mv is equal to 0.5 or 2 kg/s, a weak outflow motion is observed in the lower portion of the doorway. No such phenomenon was found in the similar simulations for the compartment fires reported in the literature[3,5]. After scrutinizing numerical results, the generation of this outflow region is closely related to the reacting flow structure inside the compartment and the forced ventilation. This will be discussed later. In the case of Mv = 0.5 kg/s, a complicated distribution of the inflow and outflow regions is formed as shown in Fig. 5a. When the ventilation rate increases to 1.0 kg/s, the inflow region is only found in the lower part. This kind of flow pattern was observed by the other numerical simulations[3,5] as well. A small outflow region is generated near the bottom of the doorway as the ventilation rate increases to 2.0 kg/s. Since the mass transfer characteristics through the doorway are very sensitive to the forced ventilation rate, the compartment fire structure must be affected accordingly.

## Flow Structures inside the Compartment

To explore the three-dimensional flow structures inside the compartment, the velocity vector distributions are plotted on different x-y and x-z planes, as shown in Figs. 6–11, respectively. Figure 6 is the velocity vector distributions on different x-z planes, viewed from y/L = 0 plane (or see Fig. 1 for the coordinates), for a ventilation rate of 0.5 kg/s. At y/L = 0.016 plane, the impingement between the jet flow and solid boundaries, i.e., the ceiling and two vertical walls, generates a slender recirculation cell near the ceiling. This ceiling recirculation is retained until it reaches the y/L $\approx$ 0.7 plane, where it disappears due to the suppression caused by a strong upward flow motion. Obviously, this upward flow motion is induced by a strong buoyancy effect on the entrained 'cold' air through the doorway. The outflow motion near the floor shown in Fig. 6(e) is generated by the recirculat-

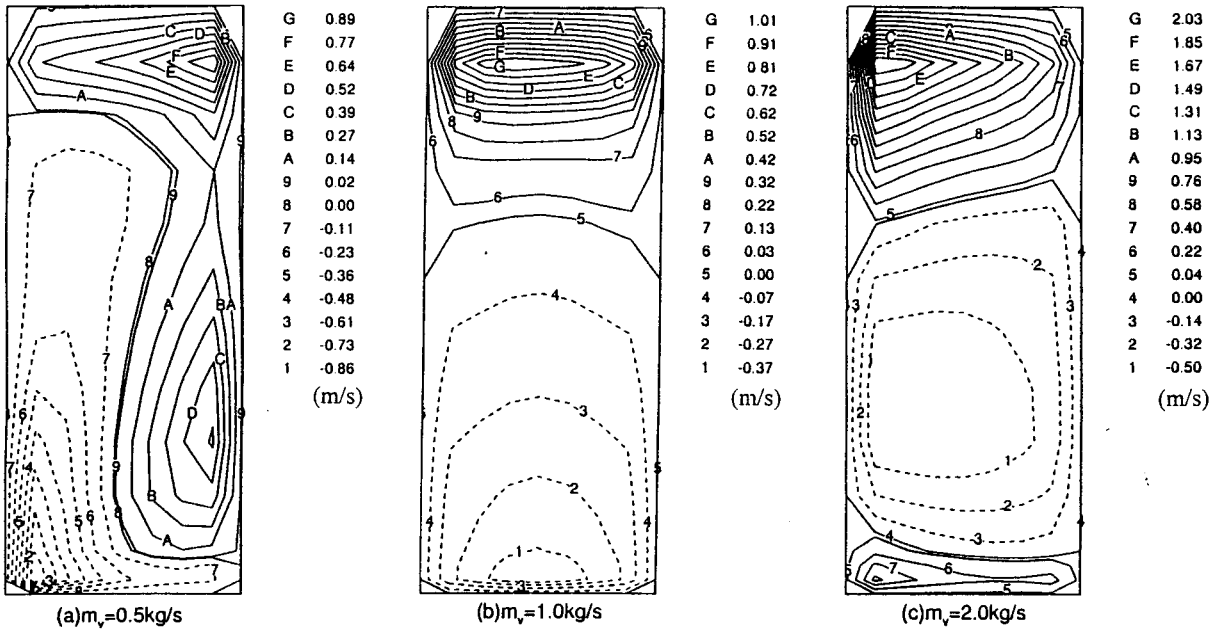


Figure 5. Normal Velocity Contours on the Doorway Plane.

ing motion on the x-y plane, see Fig. 7 for reference. In addition, near the burner outlet, a 'saddle' point of flow is produced in Fig. 6(a) due to the coupling of the wall constraint, fuel jet and near-floor recirculation flow structure. At y/L = 0.24 plane, near the ceiling, the recirculated hot flow stream, deflected downward as it impinges to the left wall in Fig. 6(b), seems to block the upward motion of 'cold' flow from the lower layer of the compartment. Two counter-rotating recirculation cells are formed in Fig. 6(c). Owing to the buoyancy effect, most of the entrained 'cold' air-flow through the doorway is deflected upward to create an upper cell. The lower cell is formed apparently owing to the entrainment effect of the entrained air-flow itself. Because of a strong downward motion near the ceiling (close to the door), the center of the clockwise rotating cell in Fig. 6(c) is shifted to the region near the floor on the y/L = 0.91 plane (Fig. 6(e)). At the same time, another recirculation cell is pushed toward the left corner of the floor.

Figure 7 shows the velocity vector plots on different x-y planes for Mv = 0.5 kg/s. Fig. 7(a) gives the flow structure near the compartment floor. In this region, the flow field is dominated by a counter-clockwise recirculation cell. As z/H is increased to 0.22, a complicated structure appears as shown in Fig. 7(b). In the inner region, the strong upward flow motion is mainly a result of the buoyant force. Near the doorway region, a formation of two recirculation cells results in a co-existence of inflow and outflow regions of the doorway plane in this horizontal level. Fig. 7(c) demonstrates that the flow is made of a clockwise recirculation cell on z/H = 0.53 plane. Therefore, the flow path of entrained air entering into the compartment is determined by the recirculation structure in this mid-layer region. The identity of this clockwise recirculation cell still remains as shown in Figs. 7(d) and 7(e). However, in the ceiling region (z/H = 0.83 and 0.92) another counter-clockwise cell is created by the interaction between the outflow motion due to the forced ventilation and the inflow motion due to the recirculation near the ceiling; see Fig. 6(a). This recirculating motion cannot maintain its strength on the z/H = 0.53 plane because of the strong upward motion (Fig. 6(b)).

The velocity vectors on different x-z planes at the ventilation rate of 1.0 kg/s are given in Fig. 8. From the comparison of Figs. 6(a) and 8(a), it can be seen that the entrainment rate of the fuel jet increases with an increase of ventilation rate. Thus a larger fire is expected in the present case compared to the case of Mv = 0.5 kg/s. The recirculation structure near the ceiling remains unchanged as Mv is varied. However, this ceiling recirculation of Mv = 1.0 kg/s remains identical in all of the x-z planes, as shown in Fig. 8. The saddle point in Fig. 8(a) is closer to the doorway

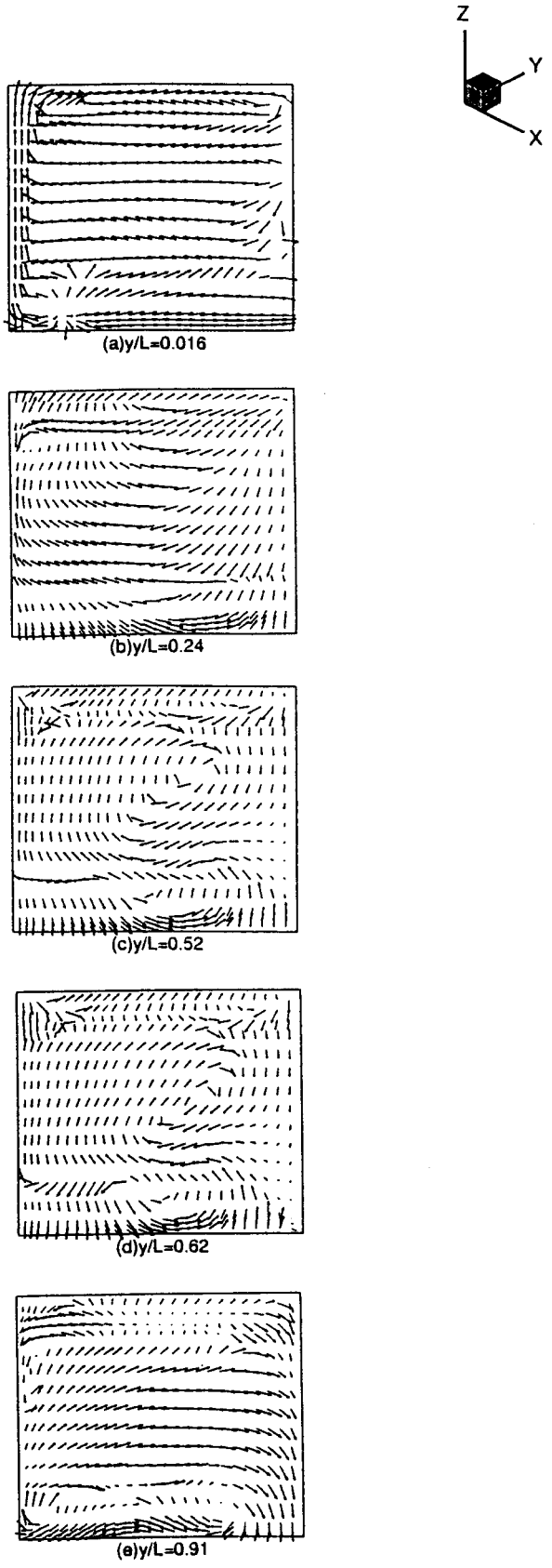


Figure 6. Velocity Vector Plots on Selected x-z Planes, Mv = 0.5 kg/s; (a) y/L = 0.016; (b) y/L = 0.24; (c) y/L = 0.52; (d) y/L = 0.62; (e) y/L = 0.91.

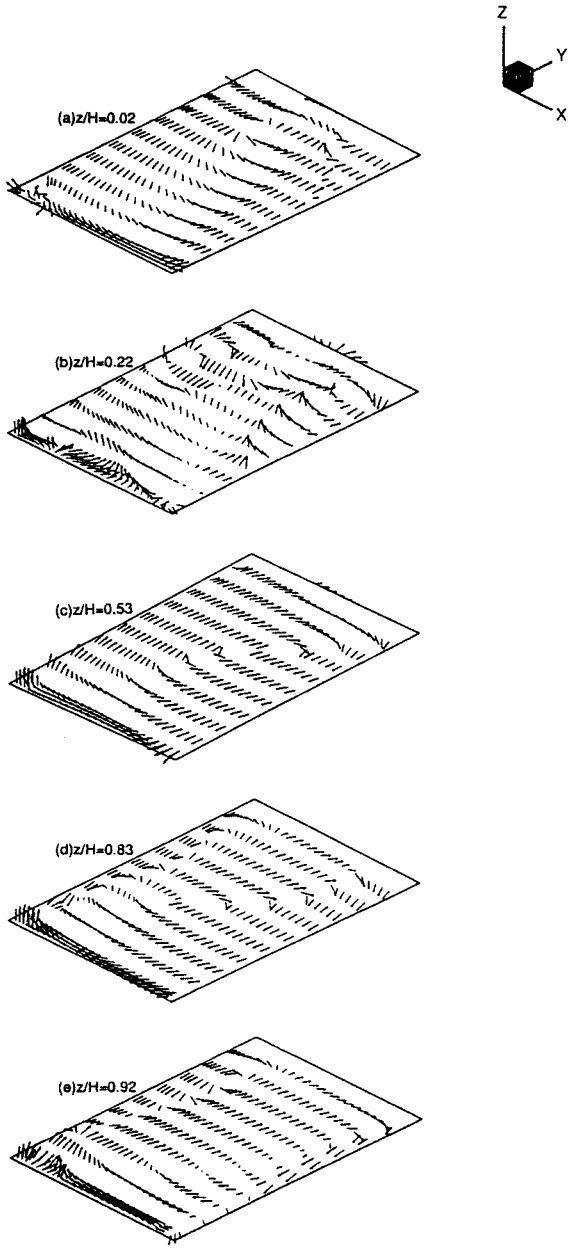


Figure 7. Velocity Vector Plots on Selected x-y Planes, Mv = 0.5 kg/s (a) z/H = 0.02; (b) z/H = 0.22; (c) z/H = 0.53; (d) z/H = 0.83; (e) z/H = 0.92.

in comparison with that of Mv = 0.5 kg/s. Because of the higher ventilation rate, the stronger upward motion in the lower layer is generated in the present case, as shown in Figs. 8(a) and 8(b). Near the doorway, this stronger upward motion interacts with the downward flow from the ceiling region and, then, generates a recirculation cell in the middle layer of the compartment on y/L = 0.24 plane. From Fig. 8(c), it is seen that the upward flow motion is still blocked by the ceiling recirculation. How-

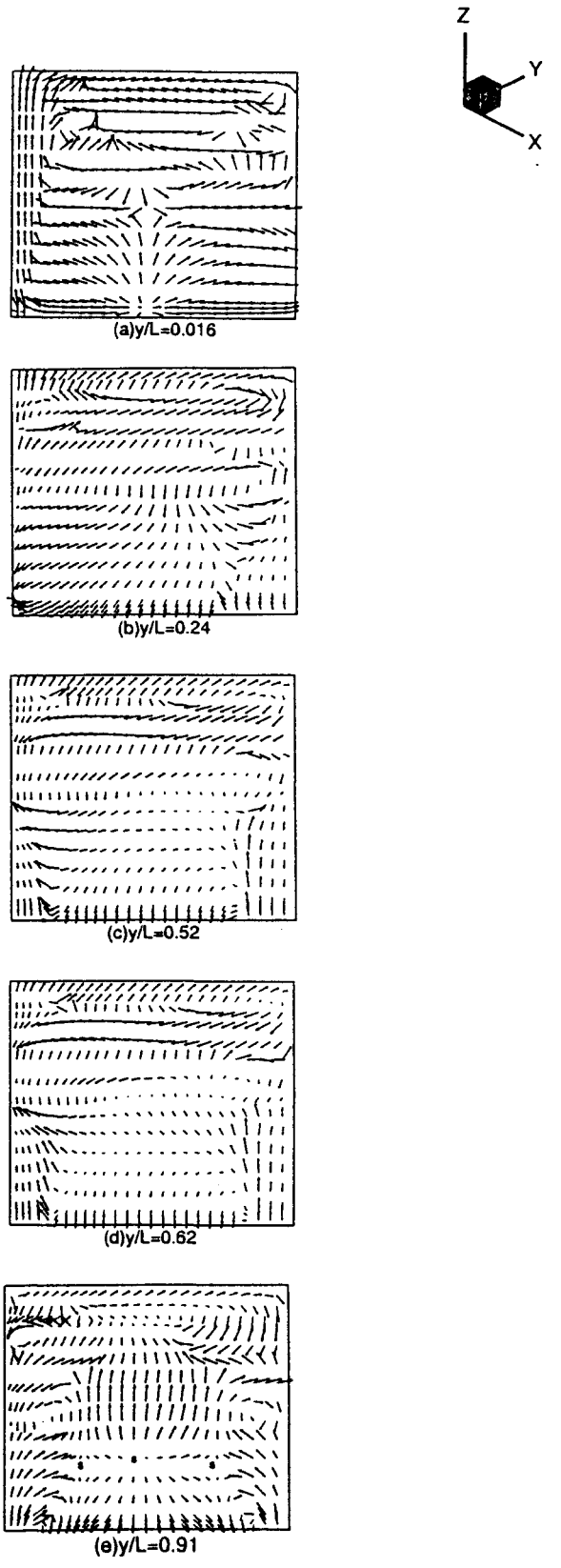


Figure 8. Velocity Vector Plots on Selected x-z Planes, Mv = 1.0 kg/s (a) y/L = 0.016; (b) y/L = 0.24; (c) y/L = 0.52; (d) y/L = 0.62; (e) y/L = 0.91.

ever, in the Mv = 0.5 kg/s case the upward flow will penetrate and suppress the ceiling recirculation on this plane. From the flow structure shown in Figs. 8(c) and 8(d), the flow entrained from the atmosphere seems not to penetrate deeply into the compartment. Consequently, only a small recirculating cell is created near the doorway plane. Besides, the lower recirculation appearing in Fig. 6(d) is not observed in the present case. It is seen from Fig. 8(e) that a very complex flow structure is established and composed of three saddle points and four recirculation cells.

Figure 9 shows the velocity vector plots on different x-y planes for Mv = 1.0 kg/s. Mainly due to the sudden expansion, the inflow mass from ambient is recirculated along two side walls so that two recirculation cells are formed on the z/H = 0.02 and 0.22 planes, shown in Figs 9(a) and 9(b). Comparing with the Mv = 0.5 kg/s case, it is found that the flow structure in the floor region is significantly changed by varying the ventilation rate. Figure 9(c) shows the velocity vector distribution on the z/H = 0.53 plane. It reveals that the entrained ambient air-flow from the lower layer will bifurcate in the mid-layer region. Part of this flow is deflected outward owing to the ventilation effect. The other part moves inward to provide the fresh oxygen to sustain combustion. Because of the stronger outflow motion, the near-doorway recirculation appearing in Fig. 7(e) is significantly suppressed such that it is barely seen in Fig. 9(e). Although centers of recirculation zones are changed with the ventilation rate, the basic flow pattern remains the same in the hot ceiling region.

Comparing with the previous two cases, velocity vector distribution on the y/L = 0.016 plane in the case of Mv = 2.0 kg/s, shown in Fig 10(a), shows a totally different flow structure. The fuel jet diffuses rapidly after injection. No recirculation structure is found on this plane. The ceiling recirculation is also observed in Fig. 10(b). In addition, a stronger downward motion of the hot layer in the left upper corner is created and recirculated, as shown in Fig. 10(b). This recirculating motion becomes dominant in the flow structure for the y/L = 0.52 and 0.62 planes. As a result, the entrained ambient fresh air follows the recirculation cell to penetrate into the deeper region of the compartment. On the y/L = 0.91

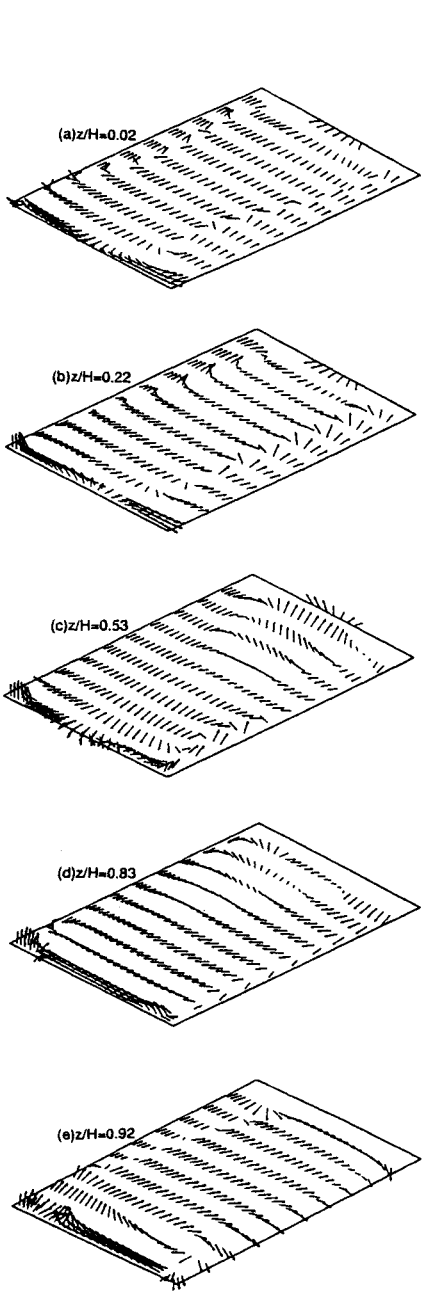


Figure 9. Velocity Vector Plots on Selected x-y Planes, Mv = 1.0 kg/s (a) z/H = 0.02; (b) z/H = 0.22; (c) z/H = 0.53; (d) z/H = 0.83; (e) z/H = 0.92.

plane, a strong recirculating structure is formed on the left upper corner of Fig. 10(e). In general, the velocity vector plots in Fig. 10 indicate that the upward motion of the entrained flow from the lower portion of the doorway possesses a dominant effect on the compartment flow structure.

Figure 11 shows the velocity vector plots on different x-y planes for the ventilation rate of 2.0 kg/s.

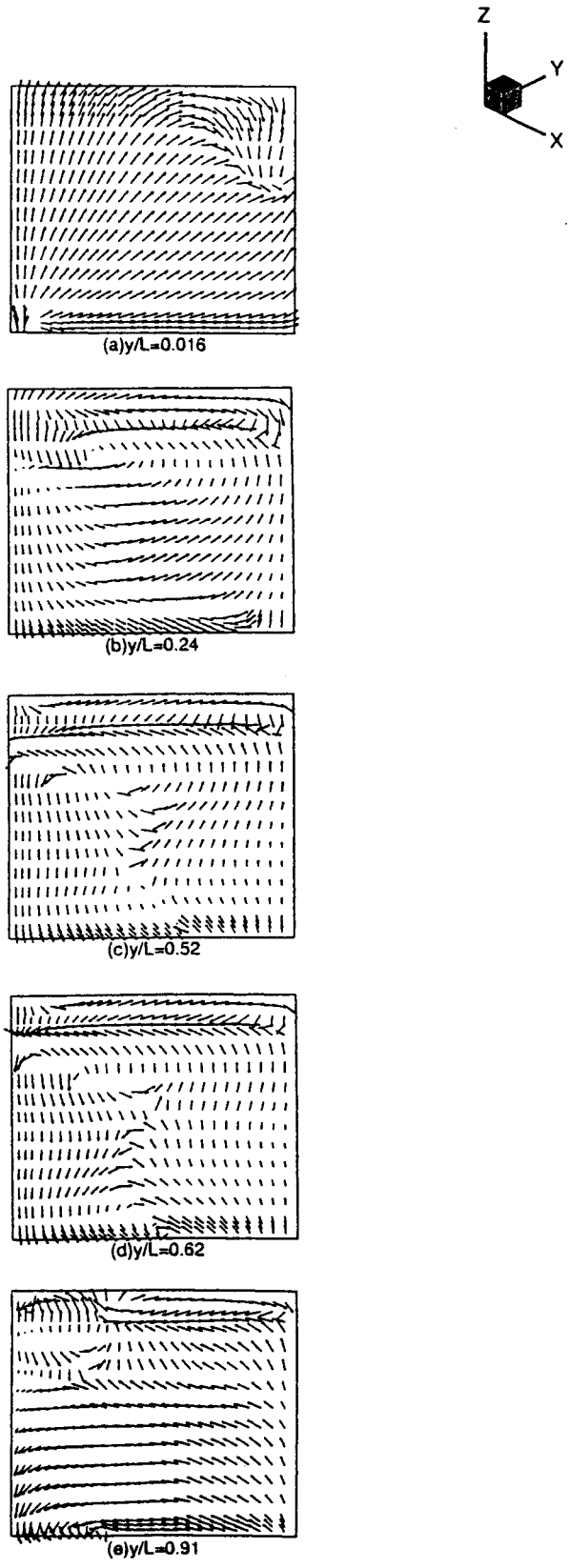


Figure 10. Velocity Vector Plots on Selected x-z Planes, Mv = 2.0 kg/s (a) y/L = 0.016; (b) y/L = 0.24; (c) y/L = 0.52; (d) y/L = 0.62; (e) y/L = 0.91.

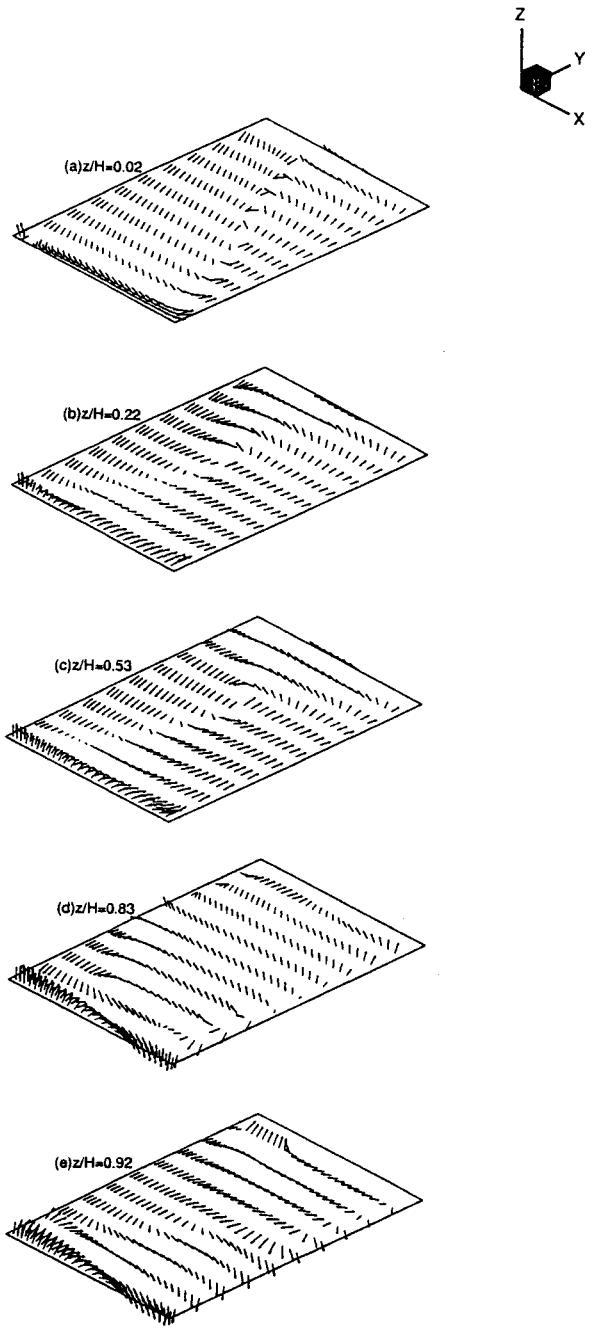


Figure 11. Velocity Vector Plots on Selected x-y Planes, Mv = 2.0 kg/s (a) z/H = 0.02; (b) z/H = 0.22; (c) z/H = 0.53; (d) z/H = 0.83; (e) z/H = 0.92.

Flow structure in the lower layer of the compartment, shown in Figs. 11(a)-11(c), indicates that only a strong counter-clockwise recirculation is established. Apparently, this one-cell phenomenon results from the strong tangential component of inflow (or outflow) velocity near the doorway plane so that the recirculation cells, due to sudden expansion created in the Mv = 1.0 kg/s case, are not formed in this case. The flow direction through the doorway plane is mainly determined by the strength and center of the recirculation cell. Under the influence of mechanical ventilation and buoyant force, the hot layer flows outward. The inflow then results in the middle layer to satisfy the mass conservation requirement on the doorway plane. Since in the middle layer the inflow acts as an air jet, having a strong upward velocity component, a local low pressure region is generated in the bottom layer. Consequently, the outflow region is formed near the floor because the recirculating outflow in the compartment can overcome the pressure gradient across the doorway. This phenomenon is clearly demonstrated in Figs. 10(b)-10(d), respectively. The velocity vector distribution in Fig. 10(d) shows that near-doorway flow has an outward velocity component because of ventilation effect. The recirculation center on this plane is shifted to the region close to the plume (or fire). A very strong downward flow is generated on the bottom corner of the figure. Due to the blockage by the door soffit, the near-doorway flow changes its direction from the z/H = 0.83 plane to the z/H = 0.92 one. In fact, this flow direction change results in a ceiling recirculation. The inflow motion of the ceiling recirculation on the z/H = 0.92 plane is so strong that the plume can only flow toward the bottom corner region of Fig. 10(e).

From the three-dimensional distributions of velocity vector given in Figs. 6–11, it is revealed that, under the interaction of the mechanical ventilation and combusting flow inside the compartment, the flow path of the entrained ambient air is drastically changed. Among these cases, the entrained ambient flow in the Mv = 1.0 kg/s case has the least penetration depth and thus the least mass transfer rate through the doorway plane.

## Temperature Distributions inside the Compartment

Since the compartment flow structure and mass transfer through the doorway are significantly changed by the ventilation rate, the fire structure and thus the temperature distribution are affected accordingly. Figures 12–14 show the temperature contours on the selected x-z planes under Mv = 0.5, 1.0 and 2.0 kg/s, respectively. From Fig. 12(a), intensive combustion is observed along the side wall and ceiling. This

phenomenon is generally observed in the room fire tests[13]. Because of the intensive reaction and strong buoyancy along the side walls, a narrow-width fire with very high temperature is generated. The quite broad hot layer found in Fig. 12(a) is mainly caused by the recirculating motion in the ceiling region. Comparing with the velocity vector distribution in Fig. 6, it is found that in the ceiling region the position of high temperature area is closely related to the location of the ceiling recirculation cell. Although steep temperature gradients, in both x and z directions, are observed on the y/L = 0.016 plane, they become smoother as y increases. Obviously, the ceiling recirculating motion in the x-y and x-z planes facilitates heat transfer in the hot layer. The clear temperature stratification phenomenon is finally observed on the y/L = 0.91 plane; see Fig. 12(d).

In comparison with the case of Mv = 0.5 kg/s, a wider fire plume with a lower flame temperature is found in Fig. 13(a); Mv = 1.0 kg/s. In addition, a thinner hot layer is generated in the ceiling region. Only a slight change in temperature distributions is found in the different x-z planes, as shown in Figs. 13(b)–13(d).

As the ventilation rate is increased to 2 kg/s, the temperature distributions on the different x-z planes are shown in Fig. 14. In general, the temperature level in the present case is lower than the other two lower ventilation rate cases because of the larger rate in mass transfer

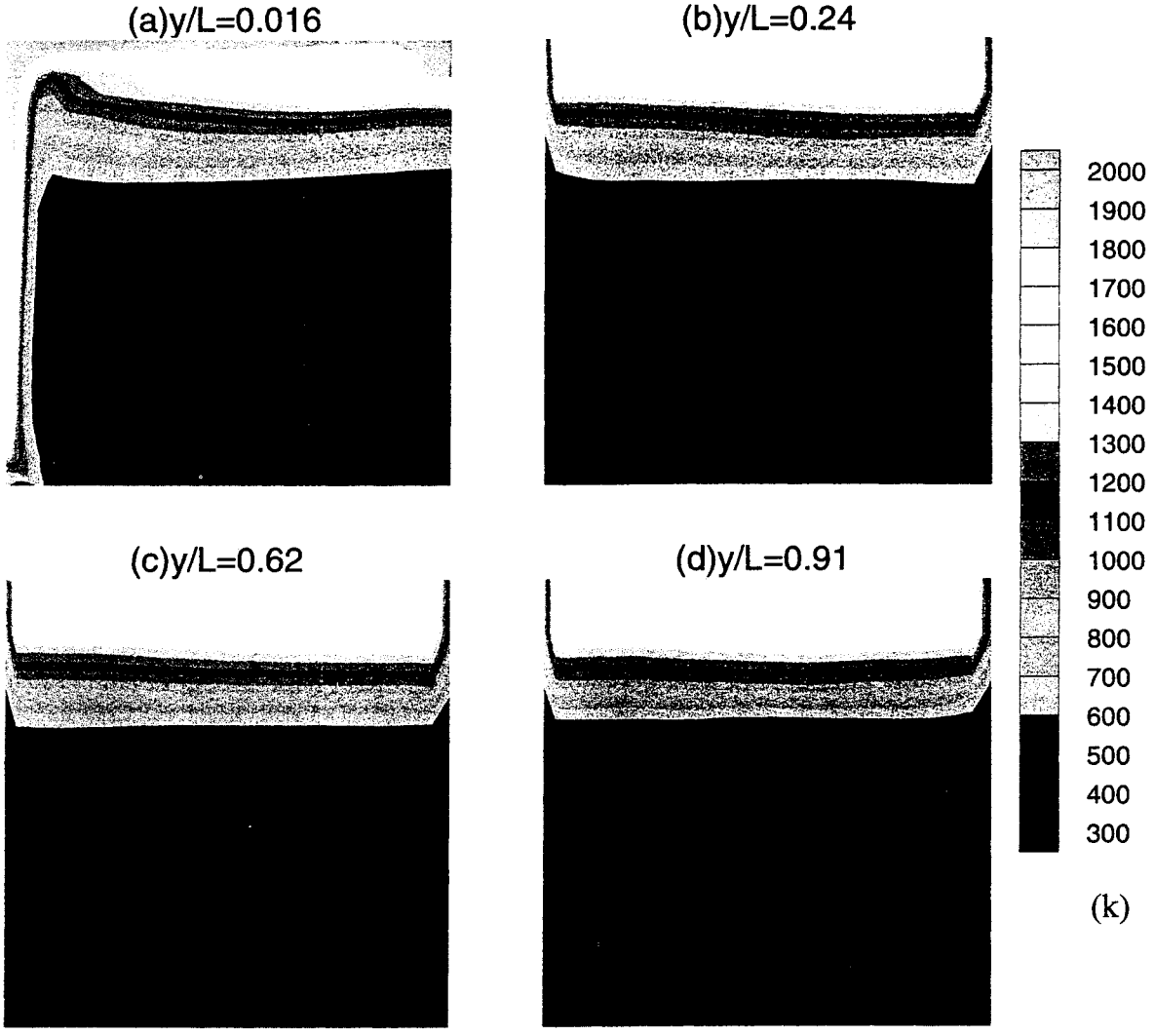


Figure 12. Temperature Contours on Selected x-z Planes, Mv = 0.5 kg/s (a) y/L = 0.016; (b) y/L = 0.24; (c) y/L = 0.62; (d) y/L = 0.91.

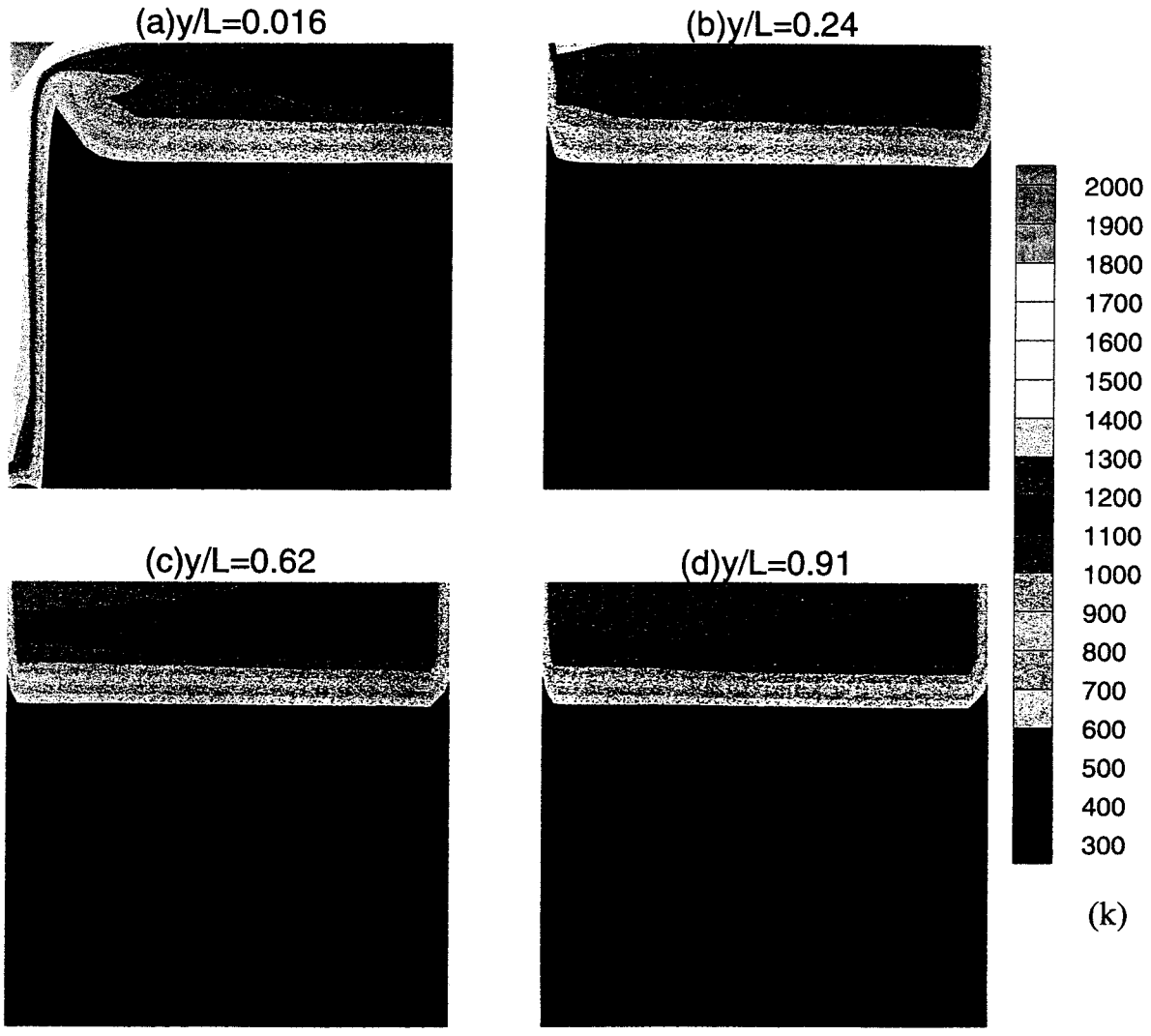


Figure 13. Temperature Contours on Selected x-z Planes, Mv = 1.0 kg/s (a) y/L = 0.016; (b) y/L = 0.24; (c) y/L = 0.62; (d) y/L = 0.91.

through the doorway plane. From Fig. 14(a), it indicates that a rapid mixing between the fuel jet and entrained ambient air results in a wider reaction zone. Besides, the cold air flow in the lower layer penetrates into the ceiling layer. The region with the highest temperature level appears in the upper left corner of Fig. 14(b). Apparently, this is because the fire plume, blocked by the inflow entrained ambient air-flow in the x direction, is deflected toward the direction with an increasing z value (height) in the ceiling region. Since there is no dominant recirculating flow structure appearing on the x-y plane in the ceiling region, non-negligible temperature gradients appear in Figs. 14(b)–14(d). Comparing with the two former cases, the stratification seems more intensive in the present case.

## Conclusions

An application of a commercial field-typed code, CFX, is conducted to simulate the ISO 9705 compartment fires with three different ventilation rates; Mv = 0.5, 1.0, and 2.0 kg/s. The computational domain consists of the compartment, the exhaust gas hood and the surrounding atmosphere. Numerical results show excellent agreement with the corresponding experimental data, except the ones near the ceiling. The discrepancy is a result of two factors; first is the fact that there was no radiation loss to the gases and conduction losses to the walls and ceiling; second is the use of a coarse grid resolution. The complicated three-dimensional compartment fire structures are described by the velocity vector plots and temper-

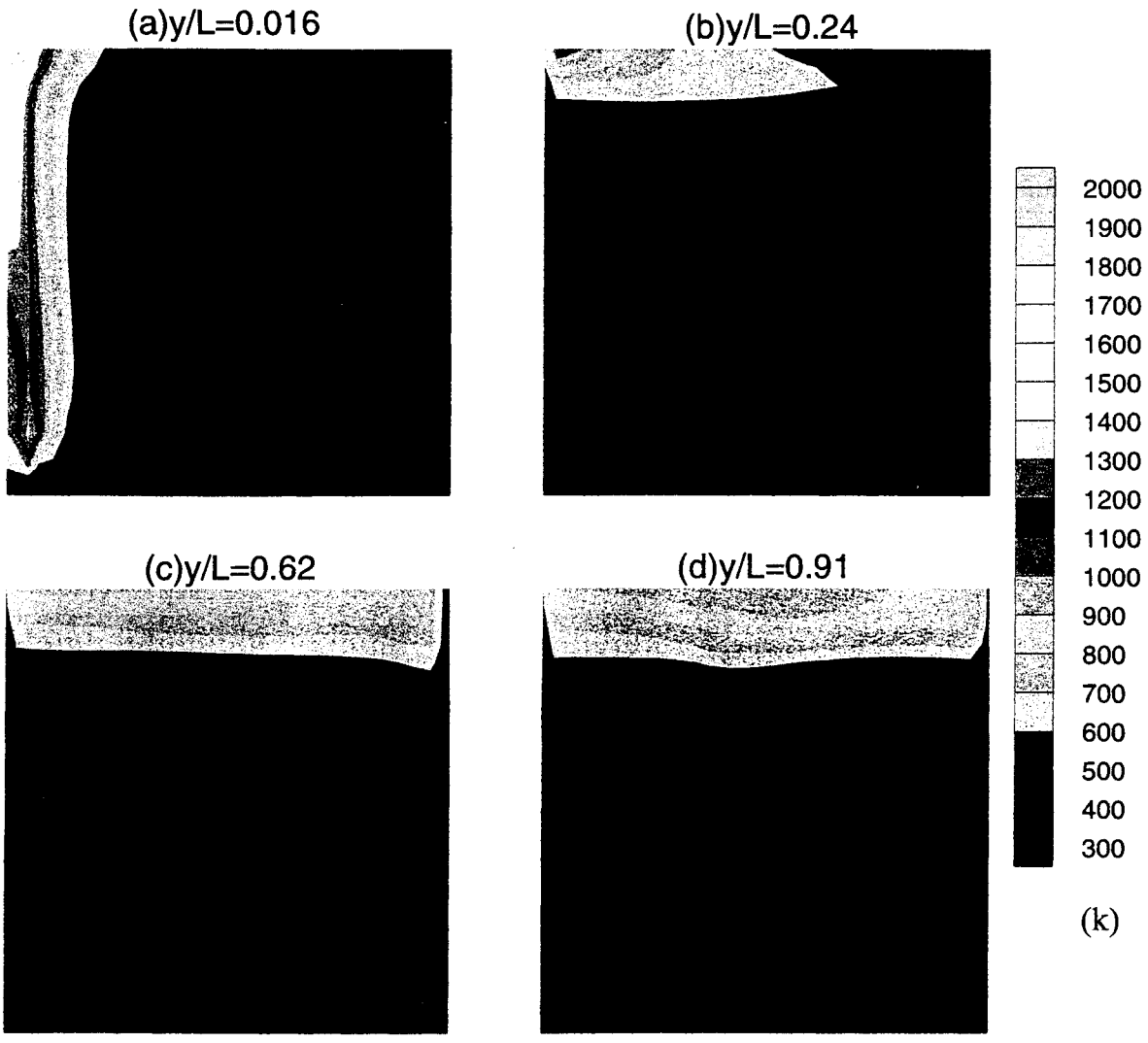


Figure 14. Temperature Contours on Selected x-z Planes, Mv = 2.0 kg/s (a) y/L = 0.016; (b) y/L = 0.24; (c) y/L = 0.62; (d) y/L = 0.91.

ature contours on the different x-z and x-y planes. It is found that the mechanical ventilation rate through the gas hood plays a dominant role on the flow path of the entrained ambient air and the reacting flow inside the compartment. Many recirculation cells are generated inside the compartment flow field. The presence of the recirculating flow pattern on the x-y and x-z planes can facilitate the mass and heat transfer in the compartment. Among the three ventilation rates, the lowest temperature is found to exist in the case with the largest ventilation rate because of the largest mass transfer rate through the doorway plane. The temperature stratification phenomenon is found away from the burner.

## ACKNOWLEDGEMENTS

Financial support of this research by the National Science Council and Architecture and Building Research Institute of the R.O.C. under projects, NCHC-85-06-001 and MOIS-850002, is greatly appreciated.

## NOMENCLATURE

| | |
|---|---|
| k | turbulent kinetic energy |
| H | compartment height (=2.4m) |
| L | compartment length (=3.6m) |
| Mv | ventilation rate (kg/s) |

s saddle point
S source term in governing equation
t time
T temperature (K)
v velocity (m/s)
W compartment width (=2.4 m)
x coordinate (m)
y coordinate (m)
z coordinate (m)

## Greek Symbols

$\Gamma$ effective exchange coefficient
$\phi$ variable
$\rho$ density
$\epsilon$ dissipation rate of turbulence energy

## Subscripts

i, j tensor index
$\phi$ variable

# REFERENCES


1. Lockwood, F.C. and Malalasekera, W.M.G., "Fire Computation: The 'Flashover' Phenomenon", *Proceedings of the 22nd Symposium (International) on Combustion, The Combustion Institute*, 1988, pp. 1319–1328.

2. Chow, W.K. and Leung, W.M., "A Short Note on Achieving Convergent Results in Simulating Building Fire Using the k-$\epsilon$ Turbulent Model", *Numerical Heat Transfer*, Part A, Vol. 17, 1990, pp. 495–501.

3. Hadjisophocleous, G.V. and Cacambouras, M., "Computer Modeling of Compartment Fires", *J. of Fire Prot. Engr.*, Vol. 5, 1993, pp. 39-52.

4. Chow, W.K. and Fong, N.K., "Application of Field Modelling Technique to Simulate Interaction of Sprinkler and Fire-Induced Smoke Layer", *Combustion Science and Technology*, Vol. 89, 1993, pp. 101–151.

5. Kerrison, L., Mawhinney, E.R., Hoffmann, N. and Patel, M.K., "A Comparison of Two Fire Field Models with Experimental Room Fire Data", *Proceedings of the Fourth International Symposium on Fire Safety Science*, Hemisphere Publishing Corp., New York, 1995, pp. 161–172.

6. Habib, A.H. and Jaluria, Y., "Turbulent Penetrative and Recirculating Flow in a Compartment Fire", *ASME Journal of Heat Transfer*, Vol. 117, 1995, pp. 927–935.

7. AEA Industrial Technology, FLOW3D User Guide, CFD Department, Harwell Laboratory, UK, 1992.

8. Wang, C.F., "The Study of Full-Scale Room Fire Test Method", Master Thesis, National Chiao-Tung University, Taiwan, 1996 (in Chinese).

9. Serag-Eldin, M.A. and Spalding, D.B., "Computations of Three-Dimensional Gas-Turbine Combustion Chamber Flows", *Journal of Engineering for Power*, Vol. 101, 1979, pp. 326–336.

10. Van Doormaal, J.P. and Raithby, G.D., "Enhancements of the SIMPLE Method for Predicting Incompressible Fluid Flows", *Numerical Heat Transfer*, Vol. 8, 1985, pp. 635–652.

11. Ho, W.C., Weng, L.C. and Chen, C.H., "Ventilation Effects on the Flow Structure in a Compartment: Cold Flow Results", *Proceeding of the 20th National Conference on Theoretical and Applied Mechanics*, Taipei, Taiwan, 1996, pp. 339–346.

12. Lewis, M.J., Moss, M.B. and Rubini, P.A., "CFD Modeling of Combustion and Heat Transfer in Compartment Fires", *Proceedings of the Fifth International Symposium on Fire Safety Science*, 1997, pp. 463–474.

13. Williamson, R.B., Mowrer, F.W. and Fisher, F.L., "Observations of Large Scale Turbulence in Corner-Wall Experiments", *Combustion Science and Technology*, Vol. 41, 1984, pp. 83–99.